ISPRS Journal of Photogrammetry and Remote Sensing 79 (2013) 199–210

Contents lists available at SciVerse ScienceDirect

ISPRS Journal of Photogrammetry and Remote Sensing

journal homepage: www.elsevier.com/locate/isprsjprs

Sensitivity of spectral reflectance values to different burn and vegetation ratios: A multi-scale approach applied in a fire affected area

Magdalini Pleniou, Nikos Koutsias *

Department of Environmental and Natural Resources Management, University of Ioannina, G. Seferi 2, GR-30100 Agrinio, Greece

ARTICLE INFO

Article history:
Received 21 April 2012
Received in revised form 16 February 2013
Accepted 22 February 2013
Available online 27 March 2013

Keywords:
Spectral properties
Sub-pixel
Burned surfaces
LANDSAT
ASTER
IKONOS

ABSTRACT

The aim of our study was to explore the spectral properties of fire-scorched (burned) and non fire-scorched (vegetation) areas, as well as areas with different burn/vegetation ratios, using a multisource multiresolution satellite data set. A case study was undertaken following a very destructive wildfire that occurred in Parnitha, Greece, July 2007, for which we acquired satellite images from LANDSAT, ASTER, and IKONOS. Additionally, we created spatially degraded satellite data over a range of coarser resolutions using resampling techniques. The panchromatic (1 m) and multispectral component (4 m) of IKONOS were merged using the Gram-Schmidt spectral sharpening method. This very high-resolution imagery served as the basis to estimate the cover percentage of burned areas, bare land and vegetation at pixel level, by applying the maximum likelihood classification algorithm. Finally, multiple linear regression models were fit to estimate each land-cover fraction as a function of surface reflectance values of the original and the spatially degraded satellite images.

The main findings of our research were: (a) the Near Infrared (NIR) and Short-wave Infrared (SWIR) are the most important channels to estimate the percentage of burned area, whereas the NIR and red channels are the most important to estimate the percentage of vegetation in fire-affected areas; (b) when the bi-spectral space consists only of NIR and SWIR, then the NIR ground reflectance value plays a more significant role in estimating the percent of burned areas, and the SWIR appears to be more important in estimating the percent of vegetation; and (c) semi-burned areas comprising 45–55% burned area and 45–55% vegetation are spectrally closer to burned areas in the NIR channel, whereas those areas are spectrally closer to vegetation in the SWIR channel. These findings, at least partially, are attributed to the fact that: (i) completely burned pixels present low variance in the NIR and high variance in the SWIR, whereas the opposite is observed in completely vegetated areas where higher variance is observed in the NIR and lower variance in the SWIR, and (ii) bare land modifies the spectral signal of burned areas more than the spectral signal of vegetated areas in the NIR, while the opposite is observed in SWIR region of the spectrum where the bare land modifies the spectral signal of vegetation more than the burned areas because the bare land and the vegetation are spectrally more similar in the NIR, and the bare land and burned areas are spectrally more similar in the SWIR.

1. Introduction

The assessment of the diverse consequences of fire activity on the environment, economy, society and atmosphere, requires a decision support system that is based on advanced and powerful monitoring tools. A critical issue affecting fire management is the lack of spatially explicit observations of fire occurrence that allow a detailed description of fire incidence. At short-term temporal scales (e.g., previous 30–40 years), tools to obtain spatially explicit information on burned areas have included field surveys, aerial photography, and satellite remote sensing (Morgan et al., 2001). The latter is an ideal alternative for collecting and processing the required information because it provides the necessary tools to gather information from Earth's surface in a relatively inexpensive and timely fashion (Koutsias and Karteris, 1998). Periodic spectral data in the visible and infrared part of the electromagnetic spectrum, acquired from various satellite sensors, offer an unlimited basic source of information. Using computer-assisted processing and interpretation, these data can contribute to a better, cost-effective, objective, and time-saving method to monitor and map areas affected by wildland fires (Koutsias et al., 1999).

Much progress has been made since satellite remote sensing of burned areas commenced almost three decades ago (Richards and Milne, 1983). Many characteristic examples of satellite remote sensing studies of burned land mapping and monitoring can be

* Corresponding author. Tel.: +30 26410 74201; fax: +30 26410 74176.
E-mail address: nkoutsia@cc.uoi.gr (N. Koutsias).

0924-2716/$ - see front matter © 2013 International Society for Photogrammetry and Remote Sensing, Inc. (ISPRS) Published by Elsevier B.V. All rights reserved.
http://dx.doi.org/10.1016/j.isprsjprs.2013.02.016

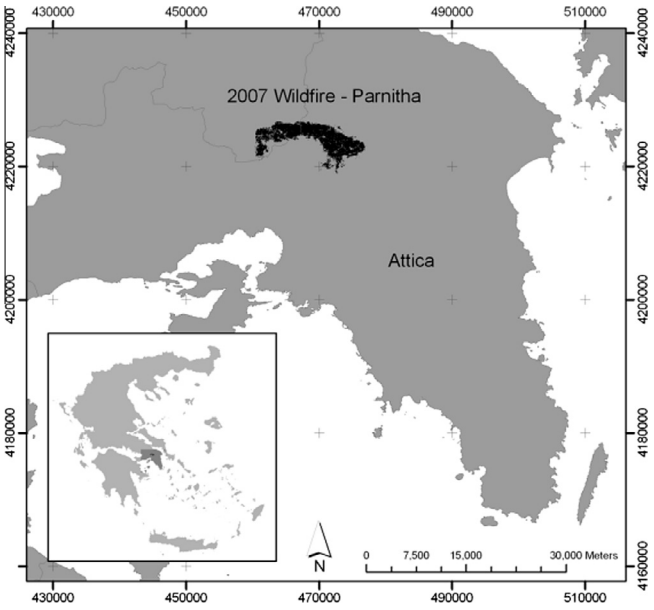

Fig. 1. Location of study area and fire scar perimeter of the 2007 wildfire in Parnitha, Attica, Greece.

found in the literature (Barbosa et al., 1999; Chuvieco and Martin, 1994; Garcia and Chuvieco, 2004; Hudak and Brockett, 2004; Justice et al., 2002; Kasischke and French, 1995; Koutsias, 2003; Koutsias et al., 2009; Laris, 2005; Pereira, 2003; Riáno et al., 2002; Roy et al., 2002; Salvador et al., 2000; Stroppiana et al., 2012, 2009, 2002; Veraverbeke et al., 2012a). Studies of burned area mapping at local, regional, and global scales have achieved very high classification accuracies (Lentile et al., 2006). However, there are still various limitations to be resolved. Therefore, burned land mapping remains an active topic of remote-sensing research (Stroppiana et al., 2012).

There is a general consensus among scientists that spectral confusion between burned areas and other land cover types may be summarized as follows (Caetano et al., 1994; Chuvieco and Congalton, 1988; Karteris, 1995; Koutsias et al., 1999; Pereira et al., 1997): (i) confusion between burned land and water bodies, especially in cases of topographically shadowed areas, recently burned surfaces, mixed land–water and water-vegetation pixels; (ii) confusion between burned land and urban areas, although this can be eliminated by masking out well-defined urban areas; (iii) confusion between burned land and shadows as a result of either irregular terrain, found especially in mountainous areas, or the presence of cloud shadows; and (iv) confusion between slightly burned land and unburned vegetation that is associated mainly with mixed pixels.

The spectral properties of fire affected areas (burned areas) are determined mainly by the removal of above-ground vegetation and the deposition of charcoal/ash as the direct result of the burning (Chuvieco and Congalton, 1988; Pereira et al., 1997; Rogan and Franklin, 2001). According to Epting et al. (2005), fire causes substantial spectral changes in the post-fire spectral signal by consuming vegetation, destroying leaf chlorophyll, exposing soil, charring stems, and altering above- and below-ground moisture. In burned areas soil reflectance is high and little vegetation remains, therefore the bare ground signature "dilutes" the vegetation signature as stated by Norton et al. (2009). All these factors are responsible for the strong modification of the spectral behavior of the "burned category pixels" compared to the pre-fire situation.

There is an agreement among scientists (Epting et al., 2005; Jensen, 2000; Koutsias and Karteris, 2000; Pereira et al., 1997; Van Wagtendonk et al., 2004; White et al., 1996) that in forest ecosystems, such as those found in the Mediterranean, a strong decrease in the reflectance of the "burned category pixels" is observed in the near- infrared region (NIR) of the spectrum of the post-fire satellite image. This reduction is due to the destruction of the leaf structure of the vegetation that reflects large amounts of the incident solar radiation in this spectral region. In addition, a strong increase in the reflectance of the "burned category pixels" is observed in the short-wave infrared region (SWIR) of the post-fire satellite image. The replacement of the vegetation layer with charcoal reduces water content, which absorbs the radiation in this spectral region. As a consequence, burned areas are expected to have higher reflectance than those of healthy vegetation.

This particular spectral behavior of burned areas in NIR and SWIR region of the electromagnetic spectrum was the basis for the successful use of the Normalized Burn Ratio (NBR) index (Key and Benson, 1999, 2006), a modification of Normalized Difference Vegetation Index (NDVI) by replacing red with SWIR, originally proposed by Lopez Garcia and Caselles (1991) who underlined the post-fire radiometric changes occurring in the SWIR, later verified by Koutsias and Karteris (2000). The replacement of the red channel with SWIR channels, that are sensitive to leaf water content because of absorption of the electromagnetic energy in this wavelength, has a long history in remote sensing (Ji et al., 2011). In fire mapping studies, NBR, which attempts to maximize reflectance change due to fire (Lozano et al., 2007), has been found to be very successful as, for example, in sagebrush steppe where the relative differenced NBR (RdNBR) provided the highest accuracy to delineate fire severity, although the Soil Adjusted Vegetation Index (SAVI) showed the highest overall accuracy in delineating burned versus unburned areas (Norton et al., 2009). Recently, Veraverbeke et al. (2012a) found that SAVI outperformed the NDVI in environments with a single vegetation type, while NDVI was more accurate in estimating vegetation cover in environments with heterogeneous vegetation layers and a single soil type. Therefore it becomes clear the importance of soil reflectance and the role of the so-called Soil Adjusted Vis that attempts to minimize the influence of the background variability (Veraverbeke et al., 2012a). Additional to NBR, Veraverbeke et al. (2012b, 2012c) proposed the SWIR-MIR and VSWIR (visible to short-wave infrared)-MTIR (mid to thermal infrared) band combinations since such data will soon be available at pixel sizes smaller than 100 m from future satellite sensors such as the Hyperspectral Infrared Imager (HyspIRI) (Veraverbeke et al., 2012b, 2012c).

The aim of our study was to explore and characterize the spectral properties of fire-scorched (burned) and non fire-scorched

Table 1
Satellite images used in the study and their characteristics.

	Date	Spatial resolution (m)	Spectral resolution
IKONOS PAN	08 July 2007	1	1, Panchromatic
IKONOS Multi	08 July 2007	4	4, Blue, Red, Green, NIR
LANDSAT TM	05 September 2007	30	6, Blue, Red, Green, NIR, SWIR (except TIR)
ASTER VNIR	20 July 2007	15	3, Green, Red, NIR
ASTER SWIR	20 July 2007	30	6, SWIR

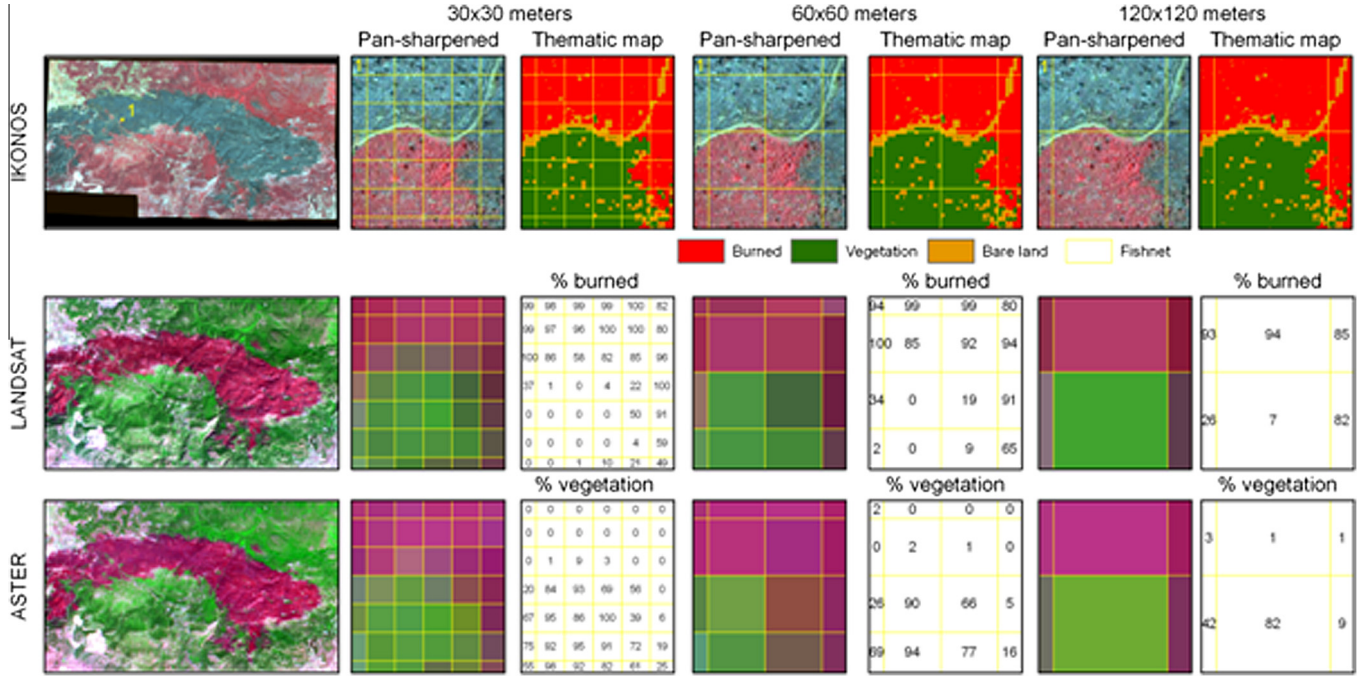

Fig. 2. Orthorectified satellite images and coarser spatial resolution data created using resampling techniques from the original data.

(vegetated) areas, as well as areas with different burn/vegetation ratios, using multisource satellite data. Most importantly, we explored all these across a multiscale-simulated image dataset, created using a spatial degradation procedure. We avoid exploring the performance of vegetation indices such as NBR or NDVI and preferred to work with the original spectral channels based on which these indices are estimated, to better understand the underlying mechanisms responsible for changes observed in the spectral reflectance values of the original spectral channels.

2. Study area and satellite dataset

In summer 2007, the year with the most destructive fires in the recent history of Greece, a large fire occurred on Mt. Parnitha (Fig. 1). Standing at an elevation of between 400 and 1400 m a.s.l, Mt. Parnitha lies 30 km NW of the city of Athens, and it is situated between 38°05′–38°15′N and 23°31′–23°51′E. The mountain of about 20,000 ha was declared as a National Park in 1961, and most human activities are prohibited in its core zone. Today, it is part of the "Natura 2000" network, designated by the European Union to protect threatened habitats and species across Europe (Panitsa et al., 2011). The elevation transect reveals the occurrence of various vegetation types, mostly dominated by *Pinus halepensis* Mill., *Quercus coccifera* L., *Pistacia lentiscus* L., *Arbutus unedo* L. and *A. andrachne* L. formations, and by phryganic (garrigue) ecosystems at low elevations. *Abies cephalonica* and *Juniperus oxycedrus* L. subsp. *oxycedrus* stands proliferate at middle to high elevations, while plateaus with grassland species are also found in forest openings (Aplada et al., 2007).

According to official statistics, the large fire which started on June 28, 2007 and was suppressed 5 days later, burned approximately 56 km^2 of land, a significant part of which lies within the National Park. The area affected by this large fire served as the case study to explore the sensitivity of spectral reflectance values at the pixel level in respect to different burn and vegetation ratios by applying a multiscale approach in the fire-affected area. For this purpose, a dataset consisting of IKONOS, ASTER, and LANDSAT (Table 1) post-fire imagery (Fig. 2) was established and used as the basic information source. Besides the satellite data, natural color aerial photographs were acquired, orthorectified, and used to establish ground-truth data.

3. Methodology

3.1. Geometric correction

All the satellite images acquired, as well as the aerial photographs, were orthorectified to compensate for geometric errors induced, for example, by the sensor itself, the Earth's rotation and curvature, and to remove image distortions created from terrain variations. For the orthorectification, a digital elevation model (DEM) at a spatial resolution of 30 m was employed. Ground-control points (GCPs) were identified on high-resolution aerial orthophotos at a scale of 1:5000 and identified also on the original uncorrected satellite and aerial images. During the orthorectification process, emphasis was placed on locating and selecting the GCPs to achieve the best possible geometric matching of all the satellite images. First, the aerial photographs were processed using already orthorectified images, then the IKONOS PAN and MULTI imagery were orthorectified, followed by the LANDSAT and ASTER imagery. During this process, all new geo-products were overlaid and checked to achieve the best possible spatial matching. The image resampling was implemented using the same constant geographic extent to ensure that each pixel of one satellite image coincided with the same pixel of the other satellite image of the same resolution (Fig. 2). For the resampling process, we used the option of nearest neighbor to avoid the smoothing effect induced by higher-order interpolations.

3.2. Radiometric and atmospheric corrections

The objective of radiometric calibration and atmospheric correction procedures is to convert satellite digital numbers to ground reflectance values (Chavez, 1996). The electromagnetic radiation collected by satellites is modified by scattering and absorption by gases and aerosols while traveling through the atmosphere from

Table 2
Accuracy report of the IKONOS classification results.

Classification	Reference					
	Burned	Non burned	Bare	SUM	User accuracy (%)	Commission error (%)
Burned	366	1	7	374	97.86	2.14
Non burned	5	390	6	401	97.26	2.74
Bare	8	9	182	199	91.46	8.54
SUM	379	400	195	974		
Producer accuracy	96.57%	97.50%	93.33%			
Omission error	3.43%	2.50%	6.67%			
Overall accuracy	96.30%					
Overall error	3.70%					

the Earth's surface to the sensor (Song et al., 2001). Therefore, depending on the application, it is necessary to correct for these atmospheric effects. Similar to Rogan and Franklin (2001), we corrected for atmospheric path radiance and converted to reflectance units using the dark object subtraction approach. The image-based approach followed is relatively simple to apply and does not require any in situ measurements or atmospheric parameters (Chavez, 1996; Schroeder et al., 2006; Song et al., 2001). This approach assumes a 1% surface reflectance for dark objects. Additionally, no atmospheric transmittance loss and no diffuse downward radiation at the surface were assumed (Rogan and Franklin, 2001). The recorded digital number (DN) values were converted to radiance at sensor and then radiance at sensor was converted to surface reflectance for each spectral channel. The conversion of DN values to at-satellite radiance depends on the sensor used. It is beyond our scope to present details on the formula used. For IKONOS we used the conversion procedure described by Thenkabail et al. (2004) and Ekercin (2007); for LANDSAT, we used that of Thenkabail et al. (2004), Schroeder et al. (2006) and Chander et al. (2009); and for ASTER, we used that of Chrysoulakis et al. (2010). During the conversion of at-sensor radiance values to the top of the atmosphere reflectance values, several parameters were taken into account, for example exoatmospheric solar irradiance (ESUN) and solar elevation angles (Chander et al., 2009). According to Chander et al. (2009), this conversion: (1) removes the cosine effect of different solar zenith angles due to the time difference between the data acquisitions, (2) takes into account the different values of the exoatmospheric solar irradiance arising from spectral band differences, and (3) corrects for the variation in the Earth–sun distance between different data acquisition dates.

3.3. Resampled satellite images

From the original imagery, we created a spatially degraded dataset from LANDSAT- and ASTER-registered images over a range of coarser resolutions using resampling techniques. This dataset can be considered similar in terms of spectral bands and radiometric sensitivity to the original imagery, thus, enabling a multiscale study of burned/vegetation spectral reflectance properties. First, we combined the ASTER VNIR channels (15 m) with ASTER SWIR (30 m) at the lower spatial resolution of 30 m. Then, we degraded the original spatial resolution by a factor of 2 each time, yielding a range of resolutions from 30 to 480 m.

3.4. High-resolution land-cover map–IKONOS imagery

In remote sensing of burned areas, it is common to evaluate coarse-resolution products by using fine-resolution ones, for example, MODIS products evaluated by LANDSAT (Morisette et al., 2005; Smith et al., 2007). In our study, the spectral properties of the areas with different burn/vegetation ratios at the pixel level from LANDSAT and ASTER were explored using a thematic map of the area created by the classification of high-resolution IKONOS imagery.

First, the panchromatic and multispectral component of the IKONOS imagery was merged using the Gram-Schmidt spectral sharpening approach (Karathanassi et al., 2007). The final pan-sharpened imagery combined the high-spatial resolution of the PAN component (1 m) with the spectral resolution of the multispectral component of IKONOS (4 channels). We then applied the maximum likelihood classification algorithm (ML) to implement a supervised classification aiming to create a three-class map, which corresponded to vegetation, burned surfaces and bare soil, by computing the probability that a given pixel belongs to a unique class. The assessment of training areas that correspond to these three classes involved the use of aerial orthophotographs and local-scale forest maps, as well as a field trip to become familiar with the study area. Finally, we estimated the accuracy of the classification output by using ground-truth data assessed in a similar way. The accuracy of the final product's assessment is summarized in Table 2.

The pan-sharpened IKONOS satellite image served as the basis for extracting the percent cover of burned areas, bare land and vegetation, at the pixel level that corresponded to the resolution of the satellite data used (Fig. 2). To achieve this we created a fishnet of 30, 60, 120, 240, and 480 m resolution that matched the geometric resolution of the LANDSAT and ASTER images and their resampled images. At each resolution, we estimated the fractions of the vegetation, burned areas and bare soil (Fig. 2).

3.5. Assessing the sensitivity of the spectral reflectance

Samples of completely "burned" and completely "vegetated" pixels were delineated, and their reflectance values at each spectral channel were extracted and used to estimate simple statistics (mean and standard deviation) to characterize the spectral properties of fire-scorched (burned) and non fire-scorched (vegetation) classes. Additionally, we also calculated the separability measure M, estimated as the ratio of the difference in mean values over the sum of the standard deviation values of the two classes. Values greater than one corresponded to good discrimination between the two classes (burned, vegetation), whereas values less than one corresponded to histogram overlapping and therefore poor discrimination. According to Pereira (1999), this index is similar to the concept of signal-to-noise ratio used to evaluate the performance of various vegetation indices when predicting fractional vegetation cover. It is also similar to the ratios of between-group variance (the difference between the mean values that represent the burned area detection signal) and within-group variance (sum of the standard deviation values that measure the level of noise) used in ANOVA and discriminant analysis (Pereira, 1999).

In addition to the identification of completely "burned" and "vegetated" pixels, we identified pixels at intermediate burn/vegetation ratios. Based on the IKONOS three-class land-cover map, we selected pixels covered by 45–55% burned and 45–55% vegetation

to define an intermediate class of "half burned" and "half vegetated" pixels at the 30 m of spatial resolution. At the 60 m and 120 m resolutions the intermediate class of "half burned" and "half vegetated" pixels included pixels covered by 40–60%, while those became 35–65% for resolutions of 240 m and 480 m. Similarly, the reflectance values of these pixels were extracted and used to estimate simple statistics (mean and standard deviation) to characterize the spectral properties of semi-burned areas. In addition, to graphically present their spectral properties, we created histogram data plots of these three classes—completely burned (100–0%), completely vegetated (0–100%), and semi-burned (half burned 45–55% and half vegetated 45–55%)—for each spectral channel of each satellite sensor for each spatial resolution. Besides the half burned-half vegetated, we also defined other proportions such as 25% burned-75% vegetation and 75% burned-25% vegetation, however, the results obtained did not differ substantively, and were therefore omitted.

Finally, linear regression models were fit to independent explanatory variables (i.e., the reflectance values for each spectral channel) to estimate the dependent response variable (i.e., percentage of burned area and percentage of vegetation at the pixel level). Regression models were fit to both satellite sensor data (LANDSAT, ASTER), to all spatial resolutions (30, 60, 120, 240, 480 m), and to different combinations of the original spectral channels (all channels, only the red-NIR-SWIR, and only the NIR-SWIR).

4. Results

4.1. Spectral properties of land cover types

The spectral signature plots of the burned, vegetation and bare land for LANDSAT and ASTER satellite sensors, based on values extracted from sampling areas located on the satellite images, is graphically presented in Fig. 3. Additionally, their mean values and standard deviation estimates, based on values extracted from the fishnet fractions of the vegetation, burned areas and bare soil, are summarized in Table 3. The spectral signatures of burned areas were compared to the other two main land cover categories to obtain a better understanding of their spectral behavior and potential discriminator ability. It was evident that the discrimination offered by the infrared spectral channels is much higher than the visible, despite the low spectral distance of bare land with the vegetation in channel TM4 and the low spectral distance of bare land with the burned areas in channel TM7. Among these, spectral channel TM7 showed the highest discrimination between the vegetation and the burned areas, followed by TM4, TM5, and TM3. The spectral behavior (presented graphically in Fig. 3) of the three main land-cover categories was also very similar in the ASTER channels. In LANDSAT TM7 band (SWIR) soil reflectance values are similar to burned area reflectance values and both are higher than the reflectance values of vegetation. These spectral properties are similar in ASTER SWIR 5-9 bands (SWIR), which corresponds to the TM7 band, with small variations as ASTER SWIR 5-9 bands have much shorter wavelengths than the LANDSAT TM7 band. In their study on the evaluation of spectral indices for burned area discrimination using MODIS/ASTER (MASTER) airborne simulator data Veraverbeke et al. (2011), demonstrated that the highest sensitivity of the longer short wave infrared (SWIR) spectral region (1.9–2.5 μm) was observed at the interval between 2.31 and 2.36 μm. In our case, the highest spectral separability between burned areas and vegetation is observed in ASTER SWIR band 8 (2.30–2.37 μm), where the separability index takes the maximum value of 3.81 (Table 4).

Table 3
Mean and standard deviation values of the vegetation, burned and bare land at each LANDSAT-5 spectral channel.

Spectral channels	Vegetation		Burned		Bare land	
	Mean	Stdev	Mean	Stdev	Mean	Stdev
Blue (TM1): 0.45–0.52 μm	0.026	0.002	0.037	0.002	0.051	0.002
Green (TM2): 0.52–0.60 μm	0.042	0.003	0.051	0.003	0.08	0.004
Red (TM3): 0.63–0.69 μm	0.041	0.003	0.062	0.004	0.109	0.006
NIR (TM4): 0.76–0.90 μm	0.173	0.009	0.104	0.007	0.209	0.005
SWIR (TM5): 1.55–1.75 μm	0.099	0.008	0.161	0.011	0.262	0.008
SWIR (TM7): 2.08–2.35 μm	0.061	0.006	0.183	0.011	0.195	0.005

4.2. Spectral signal of the semi-burned pixels

The histogram data plots of completely "burned", completely "vegetated," and "semi-burned" pixels for each spectral channel, satellite, and spectral resolution are presented in Fig. 4–7. Additionally, their separability values at the spatial resolution of 30 m are presented for both LANDSAT and ASTER channels in Table 4. From both the histogram data plots and the separability values, it is clear that in the NIR region (channel 4 in LANDSAT, channel 3 in ASTER), the category "semi-burned" (45–55% burned and 45–55% vegetation) is spectrally closer to the burned signal (separability values 0.93 and 1.03 for LANDSAT and ASTER, respectively) and spectrally further from the category "vegetation" (separability values 1.44 and 1.61, respectively). In contrast, the "semi-burned" areas were spectrally closer to the vegetation signal in the SWIR region (channel 7 in LANDSAT, channel 5–9 in ASTER). In LANDSAT, in the SWIR region of spectral channel 7 (2.08–2.35 μm), the separability value of the semi-burned area and the vegetation was 0.93 compared to the much higher 1.34 separability value between the "semi-burned" and "burned" areas. In ASTER, where the corresponding LANDSAT SWIR region (2.14–2.43 μm) is split into five channels, the separability values between the "semi-burned" and "burned" areas were much higher (1.72, 1.63, 1.71, 1.66, and

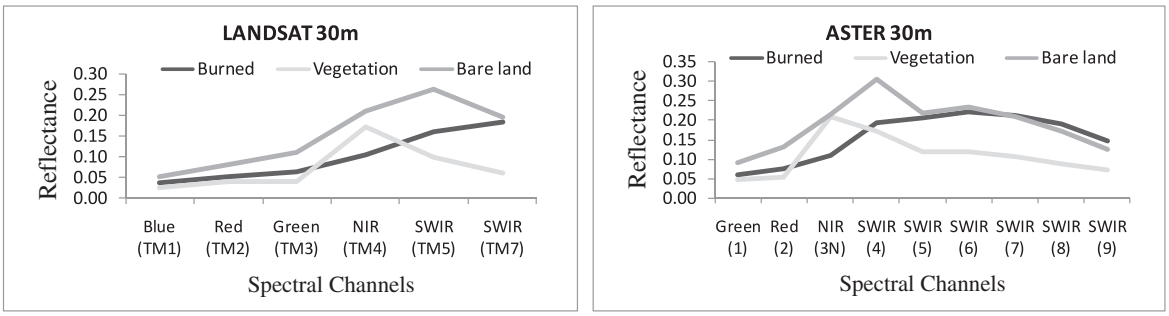

Fig. 3. Spectral signature plots of burned, vegetation, and bare land in the LANDSAT and the ASTER spectral channels.

Table 4
Separability index between main land-cover categories of each LANDSAT-5 and ASTER spectral channel.

Spectral Band	LANDSAT			Spectral band	ASTER		
	Burned/ vegetation	Semi-burned/ vegetation	Semi-burned/ burned		Burned/ vegetation	Semi-burned/ vegetation	Semi-burned/ burned
1	0.840	0.380	0.530				
2	0.331	0.070	0.303	1	0.978	0.526	0.534
3	0.918	0.724	0.298	2	1.601	1.304	0.441
4	2.216	1.443	0.929	3	2.667	1.611	1.028
5	1.082	0.485	0.630	4	0.780	0.307	0.521
7	2.611	0.934	1.336	5	2.878	1.170	1.724
				6	3.017	1.291	1.631
				7	3.495	1.115	1.710
				8	3.807	1.113	1.659
				9	3.373	1.150	1.524

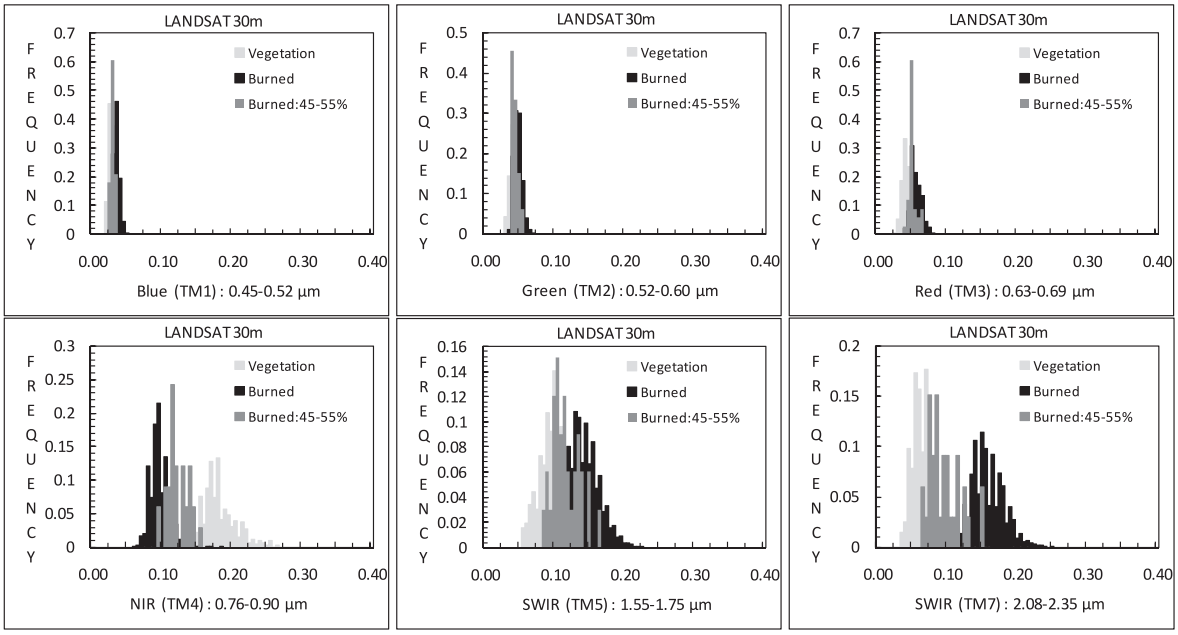

Fig. 4. Histograms of LANDSAT-5 channels for (i) completely burned pixels, (ii) completely vegetated pixels, and (iii) half burned (45–55%) and half vegetated (45–55%) pixels.

1.52) compared to those between the "semi-burned" areas and the "vegetation" (1.17, 1.29, 1.12, 1.11, and 1.15).

Finally, in the SWIR spectral region that corresponds to LANDSAT channel 5 (1.55–175 μm) and ASTER channel 4 (1.60–170 μm), the "semi-burned" areas were close to both the burned and the vegetated areas (slightly closer to the vegetation). The spectral separability of the "burned" and "vegetation" areas was just 1.0823 and 0.780 in LANDSAT and ASTER respectively, compared to 2.61 in LANDSAT channel 7, and 2.88–3.80 in the ASTER SWIR spectral channels. In addition, the separability of the "semi-burned" areas with the "vegetated" areas was 0.49 and 0.31 in LANDSAT and ASTER, respectively, whereas the separability values between the categories "semi-burned" and "burned" were 0.63 and 0.52 in LANDSAT and ASTER, respectively. Therefore, it seems that the "semi-burned" areas are almost in the center of the spectral distance between completely "vegetated" and completely "burned" areas in this spectral region.

The spectral behavior presented so far for the "semi-burned" areas in the LANDSAT and ASTER spectral channels at the original spatial resolution of 30 m was similar to that observed over the range of coarser resolutions for each sensor (Fig. 4–7). As the resolution becomes coarser, it is inevitable that the range of the burned area fraction in "semi-burned" pixels becomes wider, resulting occasionally in spectral behavior deviations.

4.3. Regression models of burn vegetation ratios

The statistics of the regression models developed to estimate the dependent response variable (i.e., the different burn and vegetation ratios) from the independent explanatory variables (i.e., the spectral channels of the satellite images) for 30 m resolution are summarized in Table 5. For the regression models developed, we used 75,441 samples at the resolution of 30 m, 19,178 samples at the resolution of 60 m, 4877 values at the resolution of 120 m, and 1296 and 342 values at the resolutions of 240 m and 480 m, respectively. The standardized coefficients of each independent variable that indicate the relative importance of each variable to explain the dependent variable are reported in the statistics. The overall fit of the models as indicated from the *R*-square value (Fig. 8) was quite high for all resolutions and for all models developed, which demonstrates the good fit of the observed values versus the predicted values. At the spatial resolution of 30 m, the general fit of the models was slightly smaller than at 60 m resolution for all cases considered, whereas after 60 m, the general fit of

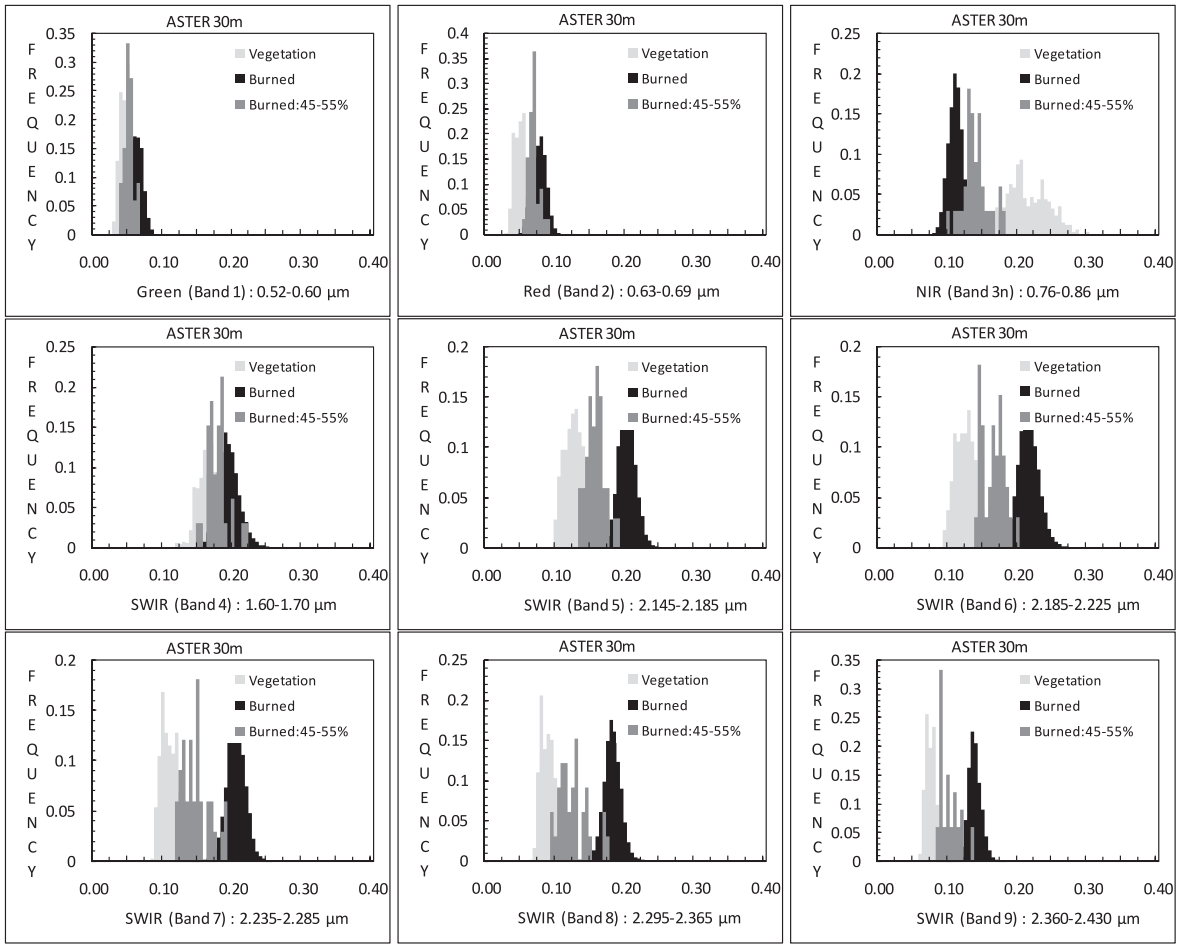

Fig. 5. Histograms of ASTER channels for (i) completely burned pixels, (ii) completely vegetated pixels, and (iii) half burned (45–55%) and half vegetated (45–55%) pixels.

the model began to decrease until 480 m where is showed the poorest fit. This unique behavior of the models general fit can be attributed to the influence of the geometric accuracy of the satellite data, which although high, was set to less than one pixel. Thus, at 30 m resolution, the uncertainty and variation created by the geometric mismatches of the satellite image was high. Therefore, it seems reasonable to observe smaller *R*-square values at a resolution of 30 m compared to a resolution of 60 m. The decrease in the *R*-square values from the resolution of 60 m to 480 m stands also appears reasonable because as the spatial resolution becomes coarser, the size of the pixel becomes larger and it is difficult to locate pure pixels. Instead, mixed ones are found with different percentages of burned, vegetation, and bare land. The spectral signal of the pixels is strongly influenced by the existence of, for example, bare soil.

From the standardized coefficients of the models developed to estimate the percentages of vegetation and burned land at the pixel level with all spectral channels (Table 5), it is clear that the best performing channels to estimate the percent of burned area are the NIR (TM4, Band 3) and the SWIR (TM7, Band 6), while the best performing channels to estimate the vegetation percentage are the NIR in both satellites (TM4, Band 3) and the red in Landsat (TM3), or the SWIR followed by red in ASTER. When analyzing the ASTER data, we have chosen Band 6 when referring to the SWIR spectral region. Band 6 has a much shorter wavelength than LANDSAT TM7 and this is probably the reason for the significance of the channel in estimating the percentage of vegetation. These findings coincide with others found in the literature where NIR and SWIR are considered to be good spectral regions for studies on burned land mapping especially for fire severity (Key and Benson, 1999, 2006), while NDVI, which consists of red and NIR spectral regions, has been found to be more accurate in estimating vegetation cover in environments with heterogeneous vegetation layers (Veraverbeke et al., 2012a). These spectral patterns, observed at high spatial resolutions (30 m), were modified at coarser spatial resolutions (especially in 240 and 480) and TM5 became important to estimate the percentage of burned area, while TM7 became important to estimate the percentage of vegetation. These spectral patterns might be explained by the spectral properties of bare land, the influence of which increases at coarse spatial resolutions because of bare land's greater prevalence. The bare land was spectrally more different than burned areas in TM5 and than vegetation in TM7 (Fig. 3). When the analysis was performed only with the three best performing channels —red, NIR, and SWIR— at a resolution of 30 m, similar relationships were found. When the analysis concerned only the NIR and SWIR regions of the electromagnetic spectrum, then the NIR ground reflectance value seemed to play a more significant role in estimating the percent of burned area at pixel level, and the SWIR ground reflectance value seemed to play a more significant role in estimating the percent of vegetation at pixel level.

5. Discussion

The findings of our research can be explained, at least partially, by the spectral properties of the main land-cover types. We

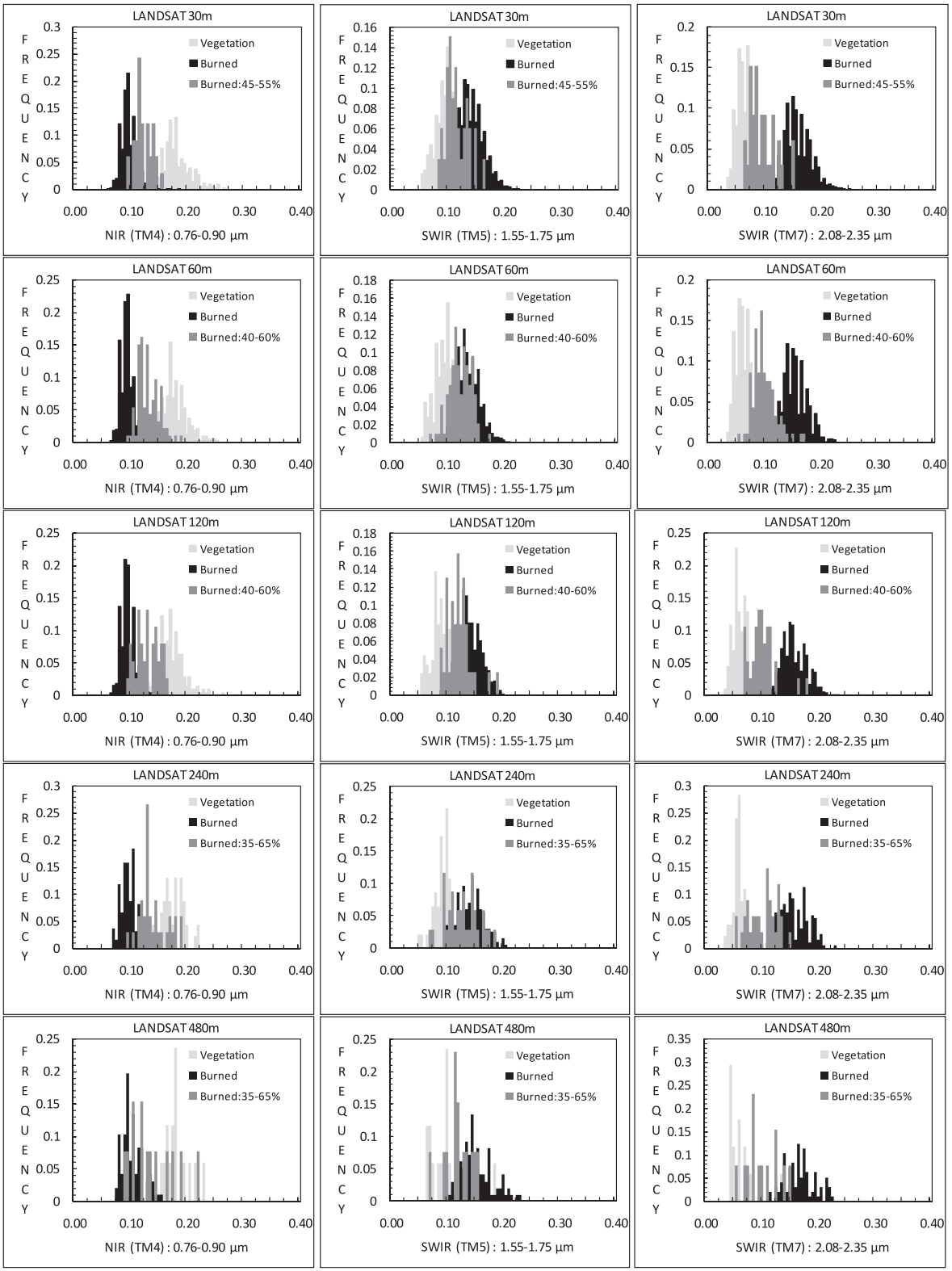

Fig. 6. Histograms of LANDSAT-5 NIR, and SWIR channels at all spatial resolutions considered in our study for (i) completely burned pixels, (ii) completely vegetated pixels, and (iii) half burned (45–55%) and half vegetated (45–55%) pixels (in higher resolutions becomes 40–60% and 35–65%).

identified two interesting patterns that influence the sensitivity of spectral reflectance values at the pixel level in respect to different burn and vegetation ratios in fire-affected areas.

The first pattern was the high standard deviation of the vegetation in the near-infrared region of the electromagnetic spectrum (TM4) and the burned areas in the short-wave infrared (TM7). Vegetation showed the highest variance in the reflectance values in the NIR band, demonstrating that factors other than cover influence the spectral response of fully vegetated areas in this region of the spectrum. Such factors could be internal parameters of the

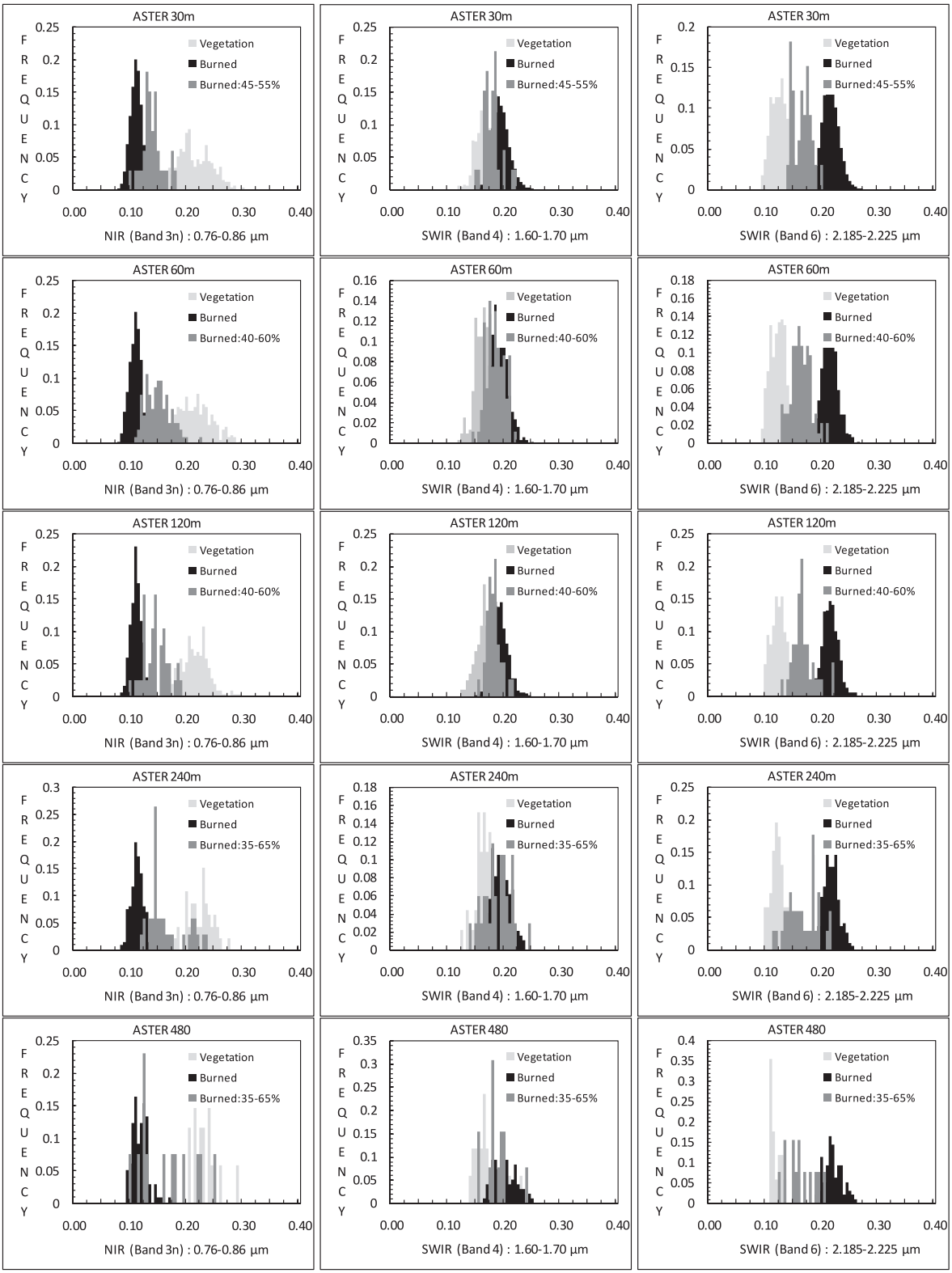

Fig. 7. Histograms of the ASTER NIR and SWIR channels at all spatial resolutions considered in our study for (i) completely burned pixels, (ii) completely vegetated pixels, and (iii) half burned (45–55%) and half vegetated (45–55%) pixels (in higher resolutions becomes 40–60% and 35–65%).

vegetation such as the leaf area index (LAI) and biomass, or external parameters such as soil reflection. Soil adjustments might be critical in burned area mapping since a substantial characteristic of fire is the alteration of the vegetation/soil balance (Norton et al., 2009) given also the high spectral variability of different soil types. From the partitioning of the vegetation spectral reflectance in the VIS, NIR, and SWIR regions of the electromagnetic spectrum in reflectance, transmittance and absorption (Fig. 9), it is evident the absorbance of vegetation in the NIR region is low, whereas reflectance and transmittance is high. This means that the amount

Table 5
Standardized coefficients (beta) of the regression models developed to estimate the dependent response variable (percent of burned, percent of vegetation) from the explanatory independent variables (spectral bands of LANDSAT, ASTER at 30 m spatial resolution).

Dependent variable	Standardized coefficients (beta)					
LANDSAT	Blue (TM1) 0.45–0.52	Green (TM2) 0.52–0.60	Red (TM3) 0.63–0.69	NIR (TM4) 0.76–0.90	SWIR (TM5) 1.55–1.75	SWIR (TM7) 2.08–2.35
Burned (30 m)	.146	−.104	−.016	−.696	−.221	.581
Vegetation (30 m)	−.014	.269	−.770	.894	−.168	−.206
ASTER		Green (Band1) 0.52–0.60	Red (Band2) 0.63–0.69	NIR (Band3N) 0.76–0.90	SWIR (Band4) 1.60–1.70	SWIR (Band6) 2.185–2.225
Burned (30 m)		.092	*−.004*	−.727	−.220	.382
Vegetation (30 m)		−.079	−.299	.691	−.014	−.375

The values in italics are not significant.
Spectral band wavelengths are given in μm.

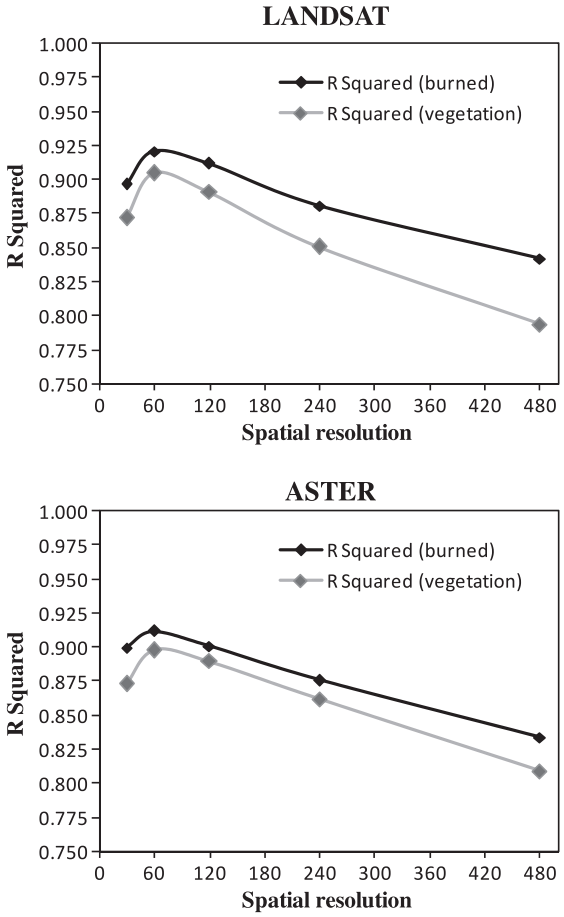

Fig. 8. R^2 as a function of spatial resolution of the satellite data.

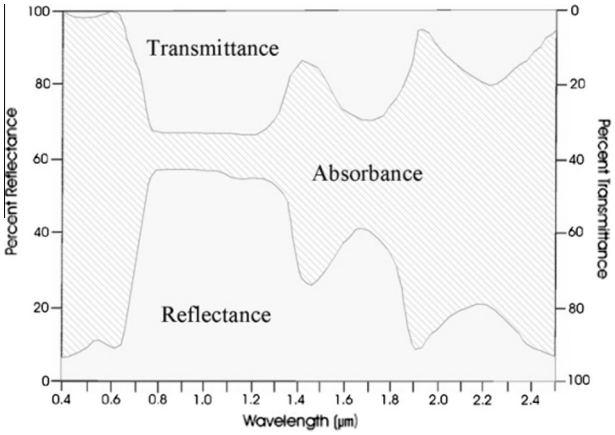

Fig. 9. Partitioning of the vegetation spectral reflectance in the VIS, NIR, and SWIR regions of the electromagnetic spectrum (reflectance, transmittance, and absorption).

of reflected energy recorded by the satellite is the result both of the direct interactions of the sun's electromagnetic energy with the upper vegetation layer that reflects part of the energy, and also with other layers beneath the upper one because a proportion of the sun's energy is transmitted to the lower vegetation layers. Therefore, besides the upper layer of vegetation, other components and parameters determine the total reflected energy recorded by the satellite sensor and increase variability (high standard deviation values of the NIR channel). Canopy reflectance, as reported by Veraverbeke et al. (2012a), presents high variability that is not only governed by vegetation amount. Other factors such as leaf optical properties or leaf angle distribution substantially alter canopy reflectance thus adding variability not imposed by the interested vegetation parameter. Accordingly, in the SWIR region, the reflectance and transmittance of the vegetation were low, and the absorbance was very high. Therefore, the first vegetation layer (e.g., 100% cover) was mainly responsible for the total reflected energy because most of the sun's energy in this region of the electromagnetic spectrum was absorbed by the vegetation, thereby minimizing the influence of other factors (e.g., soil reflectance, LAI, etc.) on the total reflected energy. Thus, it is reasonable that vegetation shows high standard deviation values in the NIR region and low standard deviation values in the SWIR region.

In contrast to the spectral patterns of vegetation, the burned areas showed the opposite behavior. In the NIR region, the standard deviation of the reflectance values was rather low compared with the much higher values in the SWIR region. Therefore, high variability in the reflectance values of completely burned areas can be expected in the SWIR region of the spectrum and low variability in the NIR region. High standard deviation estimates in the reflectance values within a spectral channel of homogenous classes, for example, when referring to completely burned or completely vegetated areas, place limitations and weaken the contribution of that channel in estimating specific parameters of that class. The high variance in the reflectance values of a class imposes internal variability not related to variations of the interested characteristic or parameter of that class. Finally, for the bare land class, the standard deviation values in the NIR (TM4) and the SWIR (TM7) regions were both similarly low (0.005). Therefore, bare land presents low variability in these two regions, whereas the opposite was observed in TM5, where the variability seems to be higher. The high variability observed in reflectance values could be one factor

explaining the reduced variance imposed in the accuracy results by the different methods applied than that imposed by factors differentiated locally when ten classification methods were applied in three test sites for burned land mapping (Mallinis and Koutsias, 2012).

The second pattern was the spectral similarity of bare land with vegetation in the NIR channel (TM4) and the spectral similarity of bare land with the burned areas in the SWIR (TM7) channel. From Table 3 which presents the mean values and the standard deviations of the three main land-cover categories in each LANDSAT-5 spectral channel, it is obvious that the land-cover pair, composed of vegetation and bare land, shows spectral similarity in the NIR region of the spectrum (TM4). Their mean spectral values were 0.209 and 0.173, respectively, which are much closer than the corresponding values between bare land and burned areas (0.209 and 0.104, respectively). This spectral similarity of vegetation and bare land in the NIR region might be critical in the reflectance value at the pixel level because the understory soil does not modify greatly the spectral signal of the pixel. In contrast, the spectral signal of bare land in the NIR region of the spectrum (TM4) was quite different from that of burned areas. Therefore, small percentages of bare land within the burned area at the pixel level might have an important effect on the reflectance value of the burned pixel. In conclusion, it seems that the existence of bare land at the pixel level modifies the spectral signal of burned areas more than the spectral signal of vegetated areas in the NIR region of the spectrum. The spectral behavior of the three main land-cover types changes in the SWIR region of the spectrum (TM7) where the bare land looks spectrally similar to burned areas and is very different to vegetation. The exact opposite was observed in the NIR region. Therefore, it seems that the existence of bare land at the pixel level modifies the spectral signal of vegetated areas more than the spectral signal of burned areas in the SWIR region of the spectrum. However, it should be kept in mind that the absorbance of electromagnetic energy from vegetation is very high in this region of the spectrum, and this minimizes the soil's influence. However, in cases where there are open patches in the canopy where the soil is exposed directly to the sun's energy, then the influence of the soil does not depend on the absorption of vegetation in this spectral region but rather on bare land spectral properties.

In post-fire assessment studies an important characteristic that might affect the success of satellite remote sensing, especially when multitemporal approaches are used, is the image acquisition date which becomes critical especially in quickly recovering Mediterranean ecosystems (Veraverbeke et al., 2010). In our study case, given that the latest satellite image was acquired on 5 September just 67 days after the fire ignition, the influence of possible regeneration that could obscure first-order fire effects as stated by Veraverbeke et al. (2010) is minimized.

6. Conclusions

The main findings of our research were: (a) semi-burned areas consisting of 45–55% burn and 45–55% vegetation were spectrally closer to burned areas in the NIR channel, whereas the same areas were spectrally closer to vegetation in the SWIR channel; (b) when bi-spectral space consisted of only the NIR and SWIR, then the NIR ground reflectance value seemed to play a more significant role in estimating the percentage of burned area at the pixel level, and the SWIR ground reflectance value seemed to play a more significant role in estimating the percentage of vegetation at the pixel level; and (c) the NIR and the SWIR were the most important channels to estimate the percentage of burned area at the pixel level, and the NIR and red were the most important channels to estimate the percentage of vegetation at the pixel level in fire-affected areas.

These findings, at least partially, are attributed to the fact that (a) completely burned pixels showed small variance in the NIR and high variance in the SWIR, whereas the opposite was observed in completely vegetated areas; and (b) bare land modified the spectral signal of burned areas more than the spectral signal of vegetated areas in the NIR region of the spectrum but, it modified the spectral signal of vegetated areas more than the spectral signal of burned areas in the SWIR region of the spectrum, because the bare land was spectrally more similar to vegetation in the NIR and to burned areas in the SWIR region.

Finally, one important observation of our research is that the observed spectral patterns were similar throughout the different spatial resolutions used (spatially degraded satellite data), however as the resolution becomes coarser (especially for 240 and 480), it is inevitable that the land cover fraction range becomes wider, thus occasionally resulting in deviations in spectral behaviors.

Acknowledgements

The research leading to these results has received funding from the European Union's Seventh Framework Programme (FP7/2007-2013) under Grant Agreement No. 243888 (FUME Project). The anonymous reviewers and the editor are gratefully acknowledged for their constructive comments on an earlier version of the manuscript that considerably improved the paper.

References

Aplada, E., Georgiadis, T., Tiniakou, A., Theocharopoulos, M., 2007. Phytogeography and ecological evaluation of the flora and vegetation of Mt Parnitha (Attica, Greece). Edinburgh Journal of Botany 64 (2), 185–207.

Barbosa, P.M., Gregoire, J.-M., Pereira, J.M.C., 1999. An algorithm for extracting burned areas from time series of AVHRR GAC data applied at a continental scale. Remote Sensing of Environment 69 (3), 253–263.

Caetano, M.-S., Mertes, L.A.K., Pereira, J.M.C., 1994. Using spectral mixture analysis for fire severity mapping. In: Viegas, D.X. (Ed.), 2nd International Conference of Forest Fire Research. ADAI, University of Coimbra, Coimbra, Portugal, pp. 667–677.

Chander, G., Markham, B.L., Helder, D.L., 2009. Summary of current radiometric calibration coefficients for Landsat MSS, TM, ETM+, and EO-1 ALI sensors. Remote Sensing of Environment 113 (5), 893–903.

Chavez Jr., P.S., 1996. Image-based atmospheric corrections – revisited and improved. Photogrammetric Engineering and Remote Sensing 62 (9), 1025–1036.

Chrysoulakis, N., Abrams, M., Feidas, H., Arai, K., 2010. Comparison of atmospheric correction methods using ASTER data for the area of Crete, Greece. International Journal of Remote Sensing 31 (24), 6347–6385.

Chuvieco, E., Congalton, R.G., 1988. Mapping and inventory of forest fires from digital processing of TM data. Geocarto International 4 (4), 41–53.

Chuvieco, E., Martin, M.P., 1994. Global fire mapping and fire danger estimation using AVHRR images. Photogrammetric Engineering & Remote Sensing 60 (5), 563–570.

Ekercin, S., 2007. Water quality retrievals from high resolution ikonos multispectral imagery: a case study in Istanbul, Turkey. Water, Air, and Soil Pollution 183 (1–4), 239–251.

Epting, J., Verbyla, D., Sorbel, B., 2005. Evaluation of remotely sensed indices for assessing burn severity in interior Alaska using Landsat TM and ETM+. Remote Sensing of Environment 96 (3–4), 328–339.

Garcia, M., Chuvieco, E., 2004. Assessment of the potential of SAC-C/MMRS imagery for mapping burned areas in Spain. Remote Sensing of Environment 92 (3), 414–423.

Hudak, A.T., Brockett, B.H., 2004. Mapping fire scars in a southern African savannah using Landsat imagery. International Journal of Remote Sensing 25 (16), 3231–3243.

Jensen, J.R., 2000. Remote Sensing of Environment. Prentice Hall Series in Geographic Information Science. Prentice Hall, Upper Saddle River, N.J..

Ji, L., Zhang, L., Wylie, B.K., Rover, J., 2011. On the terminology of the spectral vegetation index (NIR − SWIR)/(NIR + SWIR). International Journal of Remote Sensing 32 (21), 6901–6909.

Justice, C.O., Giglio, L., Koronzi, S., Owens, J., Morisette, J.T., Roy, D., Descloitres, J., Alleaume, S., Petitcolin, F., Kaufman, Y., 2002. The MODIS fire products. Remote Sensing of Environment 83 (1–2), 244–262.

Karathanassi, V., Kolokousis, P., Ioannidou, S., 2007. A comparison study on fusion methods using evaluation indicators. International Journal of Remote Sensing 28 (10), 2309–2341.

Karteris, M., 1995. Burned land mapping and post-fire effects. In: Chuvieco, E. (Ed.), Remote Sensing and GIS Applications to Forest Fire Management. Universidad de Alcala de Henares, Alcala de Henares, Spain, pp. 35–44.

Kasischke, E.S., French, N.H.F., 1995. Locating and estimating the areal extent of wildfires in Alaskan boreal forests using multiple-season AVHRR NDVI composite data. Remote Sensing of Environment 51 (2), 263–275.

Key, C.H., Benson, N.C., 1999. Measuring and remote sensing of burn severity: the CBI and NBR. In: Neuenschwander, L.F., Ryan, K.C. (Eds.), Joint Fire Science Conference and Workshop, Boise, pp. 284.

Key, C.H., Benson, N.C., 2006. Landscape assessment: ground measure of severity, the Composite Burn Index; and remote sensing of severity, the Normalized Burn Ratio. In: Lutes, D.C., Keane, R.E., Caratti, J.F., Key, C.H., Benson, N.C., Sutherland, S., Gangi, L.J., (Eds.), FIREMON: Fire Effects Monitoring and Inventory System. General Technical Report RMRSGTR-164-CD. USDA Forest Service, Rocky Mountain Research Station, Ogden, UT, pp. 1–51.

Koutsias, N., 2003. An autologistic regression model for increasing the accuracy of burned surface mapping using Landsat Thematic Mapper data. International Journal of Remote Sensing 24 (10), 2199–2204.

Koutsias, N., Karteris, M., 1998. Logistic regression modelling of multitemporal Thematic Mapper data for burned area mapping. International Journal of Remote Sensing 19 (18), 3499–3514.

Koutsias, N., Karteris, M., 2000. Burned area mapping using logistic regression modeling of a single post-fire Landsat-5 Thematic Mapper image. International Journal of Remote Sensing 21 (4), 673–687.

Koutsias, N., Karteris, M., Fernandez-Palacios, A., Navarro, C., Jurado, J., Navarro, R., Lobo, A., 1999. Burned land mapping at local scale. In: Chuvieco, E. (Ed.), Remote Sensing of Large Wildfires in the European Mediterranean Basin. Springer-Verlag, Berlin Heidelberg, pp. 157–187.

Koutsias, N., Mallinis, G., Karteris, M., 2009. A forward/backward principal component analysis of Landsat-7 ETM+ data to enhance the spectral signal of burnt surfaces. ISPRS Journal of Photogrammetry & Remote Sensing 64 (1), 37–46.

Laris, P.S., 2005. Spatiotemporal problems with detecting and mapping mosaic fire regimes with coarse-resolution satellite data in savanna environments. Remote Sensing of Environment 99 (4), 412–424.

Lentile, L.B., Holden, Z.A., Smith, A.M.S., Falkowski, M.J., Hudak, A.T., Morgan, P., Lewis, S.A., Gessler, P.E., Benson, N.C., 2006. Remote sensing techniques to assess active fire characteristics and post-fire effects. International Journal of Wildland Fire 15 (3), 319–345.

Lopez Garcia, M.J., Caselles, V., 1991. Mapping burns and natural reforestation using Thematic Mapper data. Geocarto International 6 (1), 31–37.

Lozano, F.J., Suárez-Seoane, S., de Luis, E., 2007. Assessment of several spectral indices derived from multi-temporal Landsat data for fire occurrence probability modelling. Remote Sensing of Environment 107 (4), 533–544.

Mallinis, G., Koutsias, N., 2012. Comparing ten classification methods for burned area mapping in a Mediterranean environment using Landsat TM satellite data. International Journal of Remote Sensing 33 (14), 4408–4433.

Morgan, P., Hardy, C.C., Swetnam, T.W., Rollins, M.G., Long, D.G., 2001. Mapping fire regimes across time and scale: Understanding coarse and fine-scale fire patterns. International Journal of Wildland Fire 10 (3–4), 329–342.

Morisette, J.T., Giglio, L., Csiszar, I., Justice, C.O., 2005. Validation of the MODIS active fire product over Southern Africa with ASTER data. International Journal of Remote Sensing 26 (9), 4239–4264.

Norton, J., Glenn, N., Germino, M., Weber, K., Seefeldt, S., 2009. Relative suitability of indices derived from Landsat ETM+ and SPOT 5 for detecting fire severity in sagebrush steppe. International Journal of Applied Earth Observation and Geoinformation 11 (5), 360–367.

Panitsa, M., Koutsias, N., Tsiripidis, I., Zotos, A., Dimopoulos, P., 2011. Species-based versus habitat-based evaluation for conservation status assessment of habitat types in the East Aegean islands (Greece). Journal for Nature Conservation 19 (5), 269–275.

Pereira, J.M.C., 1999. A comparative evaluation of NOAA/AVHRR vegetation indexes for burned surface detection and mapping. IEEE Transactions on Geoscience and Remote Sensing 37 (1), 217–226.

Pereira, J.M.C., 2003. Remote sensing of burned areas in tropical savannas. International Journal of Wildland Fire 12 (4), 259–270.

Pereira, J.M.C., Chuvieco, E., Beaudoin, A., Desbois, N., 1997. Remote sensing of burned areas: a review. In: Chuvieco, E. (Ed.), A Review of Remote Sensing Methods for the Study of Large Wildland Fires. Universidad de Alcala, Alcala de Henares, Spain, pp. 127–183.

Riáno, D., Chuvieco, E., Ustin, S., Zomer, R., Dennison, P., Roberts, D., Salas, J., 2002. Assessment of vegetation regeneration after fire through multitemporal analysis of AVIRIS images in the Santa Monica Mountains. Remote Sensing of Environment 79, 60–71.

Richards, J.A., Milne, A.K., 1983. Mapping fire burns and vegetation regeneration using principal components analysis. In: International Geoscience and Remote Sensing Symposium (IGARSS'83), San Francisco, pp. 51–56.

Rogan, J., Franklin, J., 2001. Mapping wildfire burn severity in southern California forests and shrublands using Enhanced Thematic Mapper imagery. Geocarto International 16 (4), 89–99.

Roy, D.P., Lewis, P.E., Justice, C.O., 2002. Burned area mapping using multi-temporal moderate spatial resolution data – a bi-directional reflectance model-based expectation approach. Remote Sensing of Environment 83 (1–2), 263–286.

Salvador, R., Valeriano, J., Pons, X., Dìaz-Delgado, R., 2000. A semi-automatic methodology to detect fire scars in shrubs and evergreen forests with Landsat MSS time series. International Journal of Remote Sensing 21 (4), 655–671.

Schroeder, T.A., Cohen, W.B., Song, C., Canty, M.J., Yang, Z., 2006. Radiometric correction of multi-temporal Landsat data for characterization of early successional forest patterns in western Oregon. Remote Sensing of Environment 103 (1), 16–26.

Smith, A.M.S., Drake, N.A., Wooster, M.J., Hudak, A.T., Holden, Z.A., Gibbons, C.J., 2007. Production of Landsat ETM+ reference imagery of burned areas within Southern African savannas: comparison of methods and application to MODIS. International Journal of Remote Sensing 28 (12), 2753–2775.

Song, C., Woodcock, C.E., Seto, K.C., Lenney, M.P., Macomber, S.A., 2001. Classification and change detection using Landsat TM data: when and how to correct atmospheric effects? Remote Sensing of Environment 75 (2), 230–244.

Stroppiana, D., Bordogna, G., Carrara, P., Boschetti, M., Boschetti, L., Brivio, P.A., 2012. A method for extracting burned areas from Landsat TM/ETM+ images by soft aggregation of multiple Spectral Indices and a region growing algorithm. ISPRS Journal of Photogrammetry and Remote Sensing 69, 88–102.

Stroppiana, D., Boschetti, M., Zaffaroni, P., Brivio, P.A., 2009. Analysis and interpretation of spectral indices for soft multicriteria burned-area mapping in mediterranean regions. IEEE Geoscience and Remote Sensing Letters 6 (3), 499–503.

Stroppiana, D., Pinnock, S., Pereira, J.M.C., Gregoire, J.-M., 2002. Radiometric analysis of SPOT-VEGETATION images for burnt area detection in Northern Australia. Remote Sensing of Environment 82 (1), 21–37.

Thenkabail, P.S., Enclona, E.A., Ashton, M.S., Legg, C., De Dieu, M.J., 2004. Hyperion, IKONOS, ALI, and ETM+ sensors in the study of African rainforests. Remote Sensing of Environment 90 (1), 23–43.

Van Wagtendonk, J.W., Root, R.R., Key, C.H., 2004. Comparison of AVIRIS and Landsat ETM+ detection capabilities for burn severity. Remote Sensing of Environment 92 (3), 397–408.

Veraverbeke, S., Gitas, I., Katagis, T., Polychronaki, A., Somers, B., Goossens, R., 2012a. Assessing post-fire vegetation recovery using red-near infrared vegetation indices: accounting for background and vegetation variability. ISPRS Journal of Photogrammetry and Remote Sensing 68, 28–39.

Veraverbeke, S., Harris, S., Hook, S., 2011. Evaluating spectral indices for burned area discrimination using MODIS/ASTER (MASTER) airborne simulator data. Remote Sensing of Environment 115 (10), 2702–2709.

Veraverbeke, S., Hook, S., Hulley, G., 2012b. An alternative spectral index for rapid fire severity assessments. Remote Sensing of Environment 123, 72–80.

Veraverbeke, S., Hook, S.J., Harris, S., 2012c. Synergy of VSWIR (0.4–2.5 μm) and MTIR (3.5–12.5 μm) data for post-fire assessments. Remote Sensing of Environment 124, 771–779.

Veraverbeke, S., Lhermitte, S., Verstraeten, W.W., Goossens, R., 2010. The temporal dimension of differenced Normalized Burn Ratio (dNBR) fire/burn severity studies: the case of the large 2007 Peloponnese wildfires in Greece. Remote Sensing of Environment 114 (11), 2548–2563.

White, J.D., Ryan, K.C., Key, C.C., Running, S.W., 1996. Remote sensing of forest fire severity and vegetation recovery. International Journal of Wildland Fire 6 (3), 125–136.